Construction and Building Materials 501 (2025) 144252

Contents lists available at ScienceDirect

Construction and Building Materials

journal homepage: www.elsevier.com/locate/conbuildmat

Impact of clay content on the fracture behavior of rammed earth: Experimental and nondestructive assessment

Fernando Ávila [a,*], Ricardo Castro [b], Álvaro Blanca-Hoyos [b], Rafael Gallego [b], Esther Puertas [b]

[a] Department of Continuum Mechanics and Theory of Structures, Polytechnic University of Valencia, Camino de Vera, 46022 Valencia, Spain
[b] Department of Structural Mechanics and Hydraulic Engineering, University of Granada, Av. Fuentenueva, 18001 Granada, Spain

ARTICLE INFO

Keywords:
Rammed earth
Fracture energy
Three-point bending test
Clay content
Nondestructive testing
FFRC
UPV

ABSTRACT

Understanding the fracture behavior of rammed earth (RE) is critical, as cracking and brittle failure often govern the structural performance and durability of rammed earth elements, particularly under extreme loading conditions. The present study investigates the fracture behavior of unstabilized rammed earth as a function of clay content, using both destructive and nondestructive testing approaches. Three-point bending tests were conducted on four unstabilized RE mixtures, with increasing clay contents of 25 %, 40 %, 65 % and 100 %, to characterize fracture behavior. Results demonstrate that increasing clay content improves stiffness, peak load and fracture energy. Despite the inherent heterogeneity of RE, results showed consistent trends and variability levels comparable to those reported in the literature. Maximum average fracture energy of 26 N/m was obtained for 65 %-clay specimens. A piecewise linear-exponential model was fitted to the load–displacement curves, with its parameters expressed as functions of clay content, enabling extrapolation to other mix designs. Nondestructive techniques (free–free resonant column and ultrasonic pulse velocity) showed good correlation with fracture energy, particularly through longitudinal natural frequency. A multivariable regression combining parameters from both nondestructive tests improved prediction accuracy ($R^2 = 0.80$), supporting the combined use of nondestructive methods for reliable assessment of rammed earth behavior. These findings contribute to improved diagnostics of existing RE structures and more effective mix design and quality control in new RE construction.

1. Introduction

Rammed earth (RE) is an ancient construction technique present since the beginning of human civilization [1]. It consists of successive layers of moist earth compacted within a temporary formwork until reaching the desired height for the wall. The soil used for rammed earth construction is typically a well-graded sand or a clayey sand, with clay acting as the only binder in the so-called unstabilized rammed earth (URE) [2,3]. If an additive, like cement or lime, is added to improve its properties, the material is referred to as stabilized rammed earth (SRE).

Rammed earth construction – particularly URE – stands out for its environmental benefits, efficiency, and use of local materials. Compared to conventional building materials like fired bricks, concrete, or steel, RE requires significantly less energy for preparation, transport, and handling, resulting in a lower carbon footprint [2,4]. URE is also fully reusable at the end of its service life, reducing material waste. RE offers good thermal performance and hygroscopic properties that help regulate indoor temperature and humidity, ensuring stable comfort throughout the year [5,6].

Given these advantages, RE construction is drawing increasing interest in recent decades, with ongoing research aimed at evaluating and optimizing its mechanical and physical performance and its durability. However, the lack of internationally unified standards and protocols for the mechanical characterization of RE has led to a wide variability in research results and, consequently, difficulty in comparisons [2,7]. Additionally, most studies have been focused on the assessment of the unconfined compressive strength and the elastic modulus, as these are relatively simple to measure through uniaxial compression tests and their values represent a standard in engineering easy to compare to other building materials. Other mechanical properties, such as tensile and shear strength, friction angle, Poisson's ratio or fracture energy are far less frequently evaluated [2,7–9].

The evaluation of the compressive behavior of rammed earth is of course important, as RE walls are meant to work mainly under compression, but several studies have pointed out that failure mechanisms

* Corresponding author.
E-mail address: favila@mes.upv.es (F. Ávila).

https://doi.org/10.1016/j.conbuildmat.2025.144252
Received 25 July 2025; Received in revised form 29 September 2025; Accepted 26 October 2025

in rammed earth structures are closely related to its tensile behavior and, especially, its tensile fracture energy (G_f) [10,11]. This parameter refers to the energy required for a crack to initiate and propagate through a material. It is an indicator of the material's resistance to crack formation and propagation, and a measure of its tensile and flexural strength [3]. Understanding fracture energy is fundamental for evaluating and improving the behavior of rammed earth under extreme and dynamic loads, as well as for developing reinforcement strategies and accurate modeling.

Since international standardization efforts have primarily focused on conventional construction materials, there are currently no specific standards for testing fracture energy in RE. In such cases, it is common practice to adapt testing procedures originally developed for concrete, as they often exhibit similar quasi-brittle behavior. Among these, the three-point bending test (3PBT) and the wedge splitting test are widely recognized and frequently used methods for evaluating the fracture behavior of concrete-like materials, and they offer potential applicability to rammed earth [12,13]. Indeed, the few studies that have examined fracture mechanics in RE have successfully employed these methods. Arto et al. [12] applied 3PBT to lime-stabilized RE with high lime contents, while Mužíková et al. [14] used the same test on small URE specimens. Corbin and Augarde [3], along with Hussaini and Toufigh [15], conducted wedge splitting tests. Other authors who required fracture parameters for RE modeling opted to estimate them empirically, without direct experimental measurements [10,16,17]. A more detailed evaluation of these prior results and a comparison with the findings of the present study are presented in the Results and Discussion section.

The particle size distribution (PSD) of soil is widely recognized as a key factor influencing the mechanical properties of RE, with clay content in particular playing a potentially significant role in fracture behavior, as it acts as the only binder material when no additives are included [9,18,19]. As previously discussed, fracture energy remains one of the least studied parameters in the structural characterization of RE, and this knowledge gap is even more pronounced when considering the influence of PSD on fracture mechanisms, with only limited scientific data available. At the time of this research, only one study has been identified that directly examines the effect of clay content on fracture energy, highlighting the relevance and novelty of the present work. That study [14] investigated the influence of different types of clay on the fracture energy of URE, using 3PBT on unusually small, unnotched prismatic specimens with a maximum aggregate size of 4 mm, and clay contents varying in a narrow range between 14.2% and 27.6%. The results showed that, for illitic clay, G_f increased with clay content. While that study addressed an important variable – the type of clay – it presents several limitations, including the restricted clay content range, small specimen size, absence of notches, and neglect of self-weight effects. In this context, the current study aims to expand knowledge of RE fracture behavior by exploring the influence of clay content across a broader range. The use of larger, notched specimens in accordance with international testing standards, along with carefully controlled compaction energy based on Proctor methods, enhances the representativeness and reproducibility of the findings.

Additionally, the present study investigates the possibility of estimating the fracture properties of rammed earth using nondestructive testing (NDT) methods. These techniques are becoming increasingly relevant, as they enable the evaluation of the material properties without damaging the sample, which is particularly valuable advantage when dealing with heritage structures or inspecting heterogeneous materials like RE. Among the various NDT methods, ultrasonic pulse velocity (UPV) is the most commonly cited in the RE literature. It has been successfully used to estimate the elastic properties of both unstabilized [20,21] and stabilized [22,23] rammed earth samples. Another promising technique is the free–free resonant column (FFRC) method, in which a prismatic specimen is excited to identify its natural frequencies, which are then correlated with the mechanical properties.

Table 1
Clay content, optimum moisture content (OMC) and maximum dry density (MDD) of the soil mixtures.

Soil	Clay [%]	OMC [%]	MDD [kg/m^3]
A	25	8.4	2020
B	40	7.7	2160
C	65	10.8	1930
D	100	15.3	1750

While this technique has been successfully applied to building stones and concrete [24–26], it was originally developed for cohesive and stabilized soils [27,28], so its application on RE is promising, even though it has not yet been explored in the literature.

Therefore, in summary, the aim of this study is to investigate the fracture behavior of unstabilized rammed earth as a function of its clay content, combining destructive and nondestructive testing methods. By performing three-point bending tests and applying a simplified fracture model, the study seeks to quantify the effect of clay content on key fracture parameters, particularly fracture energy. Additionally, the research explores the use of nondestructive techniques – free–free resonant column and ultrasonic pulse velocity – to predict fracture behavior, with the goal of enabling more efficient assessment of existing structures and supporting quality control in new construction.

2. Materials and methods

2.1. Materials

For this study, four series of samples – A, B, C and D – were manufactured, each one with a different particle size distribution, achieved mainly by varying the clay content in the mixture. In URE, clay serves as the sole binder, making its role crucial for the material's mechanical performance. According to the European Soil Classification System (EN ISO14688-2) [29], Soil A (25% clay) is classified as clayey sand, Soil B (40% clay) as gravelly clayey sand, Soil C (65% clay) as sandy clay, and Soil D as pure clay (100% clay). Fig. 1 presents the PSD of the four soil types used in this study.

Proctor tests were conducted on all four soils to determine their optimum moisture content (OMC), which is defined as the water content that results in the maximum dry density of the soil for a certain compaction energy. The tests were performed following ASTM D1557-12 [30], and the results are presented in Table 1. The values obtained align with those commonly reported in scientific studies on the mechanical properties of URE [2].

2.2. Methods

2.2.1. Three-point bending tests

Five prismatic samples were manufactured for each series by uniformly mixing the soil with water at a percentage equal to the OMC. The mixture was then poured into a mold and compacted in three layers, applying the same compaction energy per unit volume and using the same rammer specified in the Proctor standard. Previous studies [10] have shown that applying the Proctor methodology to manufacture rammed earth samples enhances specimen homogeneity and reduces dispersion in their mechanical properties. Immediately after compaction, the mold was removed, and the samples were placed on wire racks to cure for 28 days under constant ambient conditions.

The fracture energy of the material was experimentally evaluated through three-point bending tests, a widely used method for assessing the flexural and tensile behavior of materials. In the absence of specific standards for 3PBT on rammed earth samples, the tests were conducted following the European standard for concrete specimens (EN 14651) [31] and the recommendations of the International Union of Laboratories and Experts in Construction Materials, Systems, and

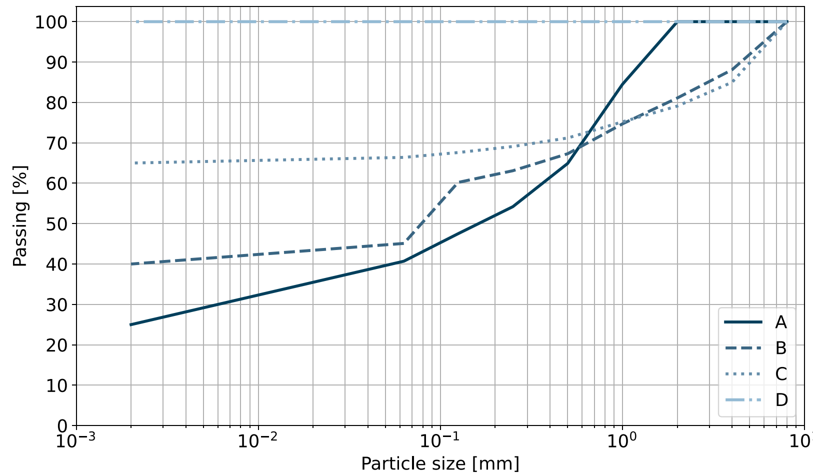

Fig. 1. Particle size distribution of the soils.

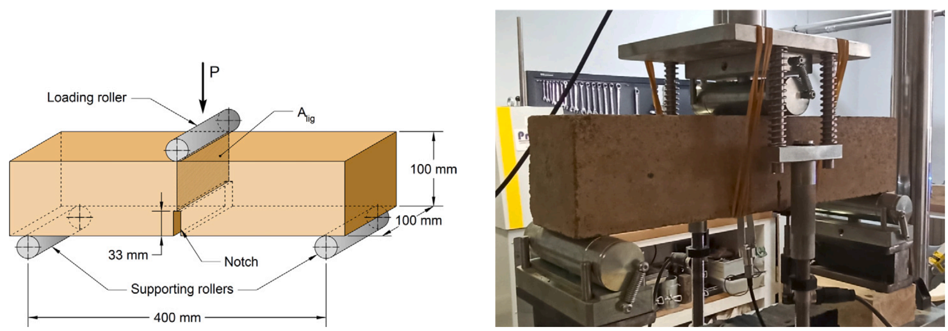

Fig. 2. Three-point bending test: (a) setup scheme and dimensions, and (b) URE specimen during testing.

Structures (RILEM) for the "determination of the fracture energy of mortar and concrete by means of three-point bend tests on notched beams" [32]. These standards and guidelines have already been successfully applied by Arto et al. [12] to analyze the fracture behavior of lime-stabilized RE samples.

The specimens had dimensions of (100×100×450) mm, allowing for a span of 400 mm between the supports. Although these dimensions are slightly smaller than those specified in concrete standards, they comply with RILEM recommendations and are consistent with the practical experience reported by Arto et al. for rammed earth samples. Once the specimens were cured, a notch was cut in the lower central part of each sample using a disk saw to a depth equal to 1/3 of the specimen's height (i.e. 33 mm). The notched samples were then positioned on the two roller supports, spaced 400 mm apart. The test was carried out by applying a vertical load P at the center of the top face of the beam, with an initial displacement rate of 0.09 mm/s. To compensate for the self-weight of the specimen, elastic bands were employed. Fig. 2(a) presents a schematic of the 3PBT setup, and Fig. 2(b) shows one of the RE specimens during testing.

Crack mouth opening displacement was monitored using a clamp transducer, while the vertical displacement at midspan was measured with a linear variable displacement transducer (LVDT) mounted on a rigid frame coupled to the specimen.

The fracture energy (G_f [N/m]) of the specimen was calculated using the work-of-fracture method [32], defined by Eq. (1):

$$G_f = \frac{W_f}{A_{lig}} \tag{1}$$

In this expression, A_{lig} denotes the ligament area, i.e., the remaining cross-sectional area after the notch is cut (see Fig. 2(a)), and W_f represents the work of fracture, equal to the area under the load–displacement (P-δ) curve. According to the correction method proposed by Elices et al. [33], to obtain the actual fracture energy of the material, it is necessary to account for the energy associated with the unrecorded tail of the P-δ curve ($\Delta W_{f,tail}$). Therefore, the corrected work of fracture to be used for the calculation of G_f in Eq. (1) must be obtained as $W_f = W_{f,test} + \Delta W_{f,tail}$. This additional term can be estimated using Eq. (2):

$$\Delta W_{f,tail} = \frac{BSA}{2\delta_f} \tag{2}$$

where B is the width of the cross section of the specimen, S is the span between the supporting rollers, A is the slope of the M-θ^2 plot (bending moment vs. squared rotation angle), calculated as detailed in [33], and δ_f is the vertical displacement at midspan at the end of the test.

2.2.2. Nondestructive tests: FFRC and UPV

Just before cutting the notch for the conduction of the 3PBT, the RE specimens were subjected to two different nondestructive analyses: free–free resonant column test and ultrasonic pulse velocity tests. The aim was to explore potential relationships between these NDT measurements and the fracture behavior of the samples.

The free–free resonant column technique allows determination of material's dynamic elastic properties by mechanically exciting a test specimen of known geometry. In this study, tests were performed following the impact resonance method defined in ASTM C215 [34]. The RE specimens, supported as described in the standard, were struck with a small impactor, and response was captured by a lightweight accelerometer attached to the sample. The signal was then amplified and processed through a waveform analyzer using Fourier transform to identify natural frequencies associated with resonance. By adjusting the placement of both the impact and sensors, transverse, longitudinal, and torsional resonant frequencies were recorded.

The ultrasonic pulse velocity method is based on measuring the propagation speed of acoustic waves through the specimen, which depends on its density and stiffness. The procedure followed the guidelines of EN 12504-4 "Testing concrete in structures - Part 4: Determination of ultrasonic pulse velocity" [35]. Two transducers (emitter and receiver) were coupled to opposite faces of the RE specimen using coupling gel to ensure proper transmission. Once the pulse was emitted, the time it took to travel through the material was recorded using a signal acquisition module. By combining this time measurement with the known distance between the transducers (mounted in a direct transmission configuration), the wave propagation velocity was calculated for each specimen. UPV measurements were conducted on each specimen along the longitudinal direction, as well as at three points across the transverse direction (near both ends and at the center).

Equipment for the FFRC tests comprised an impact hammer Brüel & Kjaer model 8206-003 (voltage sensitivity 1.14 mV/N; full-scale force range 4 448 N; maximum compression force 8 896 N; effective seismic mass 100 g; maximum frequency 600 kHz), two piezoelectric accelerometers Brüel & Kjaer Delta Tron model 4514-B-001 (titanium hexagonal head; voltage sensitivity 100 mV/g; measuring range 50 g; transverse sensitivity < 5%), and a 12-channel input module LAN XI PULSE model 3053-B-120. UPV measurements were performed using a Controls ultrasonic tester model 58-E0048, with a frequency range of 54 kHz, in accordance with standard UNE-EN 12504-4 [35].

3. Results and discussion

3.1. Three-point bending tests

The fracture behavior of the rammed earth samples was first analyzed through the load–displacement curves obtained from the 3PBT (Fig. 3). In all specimens, the mechanical response was consistent with several studies and experiences of quasi-brittle materials subjected to flexural loading [36,37]. Specifically, the curves exhibited an initial nearly linear ascending branch up to the peak load, followed by a descending softening branch with a progressively decreasing slope.

It can be observed that increasing clay content results in higher initial stiffness, greater peak load (P_{max}), and a more extended softening branch before final failure. The increase in peak load is particularly remarkable in Series C and D specimens, 65% and 100% clay, respectively. However, for the D specimens, the post-peak behavior could not be properly recorded due to sudden brittle failure occurring shortly after reaching P_{max}, which prevented the full capture of the softening branch. Although the dispersion of the key parameters is evaluated in detail later in this section, the P–δ curves already reveal a consistent fracture behavior within each series, with more notable variability observed only for Series B samples near the peak load.

The numerical results derived from the three-point bending tests are summarized in Table 2, including the fracture energy, calculated as detailed in the previous section. These results show a clear influence of clay content on the fracture strength and behavior of the rammed earth specimens. As the clay percentage increased from 25% to 65%, both peak load and fracture energy values generally improved. Series C, with 65% clay, demonstrated the highest total fracture energy (26.3 N/m), along with the largest final crack openings (0.711 mm), indicating a greater capacity for energy absorption and post-peak deformation. In contrast, Series A (25% clay) exhibited lower fracture energy (16.0 N/m) and smaller final crack opening (0.43 mm).

For the specimens with 100% clay content (Series D), although the highest peak loads were recorded (mean of 820 N), their behavior was significantly more brittle. In fact, as previously noted, the softening branch of the P–δ curve could not be captured due to sudden failure occurring shortly after peak load, making it impossible to determine the total fracture energy. Consequently, Series D was excluded from the full fracture energy-related analysis. However, to enable a comparative assessment that includes these specimens, a partial fracture energy, G_f^*, was defined as the fracture energy from the beginning of the test to the peak load.

It is important to note that the 100% clay mixture (Series D) does not reflect practical formulations of RE. Its inclusion in the experimental program was intended to provide an upper bound for clay content, offering a clearer view of its role in fracture behavior. While not representative of construction practice, this extreme case proved useful for highlighting the brittle response of pure clay and for testing the limits of the proposed fitting model described in Section 3.2.

Excluding the all-clay samples, the results from the 3PBT indicate that higher clay contents tend to enhance both flexural strength and fracture toughness in URE specimens. While pure clay samples can yield high peak strength, they lack the ductility required for desirable post-peak behavior, limiting its suitability for structural applications where energy dissipation and deformation capacity are critical.

It is challenging to directly compare the results of the present study with those available in the existing literature, due to the scarcity of studies focused on the fracture behavior of RE, as well as the variability in manufacturing and testing procedures and in the material compositions. Hussaini & Toufigh [15] conducted wedge splitting tests on URE specimens with 5% clay content, obtaining an average G_f of 20 N/m. In contrast, Corbin & Augarde [3] reported significantly lower values of 1.5 N/m using the same testing technique on samples with 30% clay. Other authors [16,17] proposed estimating G_f indirectly as 0.029 f_t, where f_t was the tensile strength derived from diagonal compression tests, resulting in G_f values between 4 and 11 N/m for URE with clay contents equal to 11% and 30%. Similarly, Bui et al. [38] adopted a G_f value of 12 N/m, estimated via an empirical formula proposed by the CEB-FIP Model Code 1990 [39], although the clay content in their specimens was not specified.

The only study that evaluated the fracture energy of unstabilized rammed earth using 3PBT is that of Mužíková et al. [14], who reported an average G_f of approximately 4 N/m for URE specimens with 25% clay. However, it should be noted that the samples were particularly small (40 × 40 × 160 mm), and the study focused on high water-clay ratios, which may have significantly influenced the results. Other authors have conducted 3PBT, but on stabilized RE specimens. For example, Arto et al. [12] measured G_f values of 23 and 34 N/m for lime-stabilized RE with 4:1 and 3:1 soil–lime ratios, respectively. Lenci et al. [40] also tested fiber-reinforced RE in 3PBT, but did not calculate fracture energy explicitly.

Overall, a direct comparison between the present results and prior studies remains challenging due to differences in testing procedures, specimen geometries, compaction protocols, and material compositions. Previous studies rarely addressed how variations in particle size distribution or clay content influence the fracture behavior of unstabilized rammed earth. By systematically evaluating a wider range of clay contents and controlling compaction with a standardized Proctor method, the obtained results provide new insights into the role of clay as the primary binder in URE and its effect on both peak load and fracture energy. Despite the inherent heterogeneity of earthen materials, the measured fracture energy values for specimens with typical clay contents (Series A and B) fall within the broad range reported in literature for URE (i.e., from 2 to 20 N/m [2]), confirming that the experimental results are consistent with expected behavior while highlighting the added value of analyzing the influence of soil granulometry. This combination of controlled experimental methodology and systematic variation of clay content allows for a more nuanced understanding of RE fracture mechanisms.

Regarding the variability observed in the results, particularly for fracture energy and notch opening, it can be largely attributed to the intrinsic heterogeneity of RE, a well-documented characteristic of this material [2]. In the present study, coefficients of variation (CV) for G_f

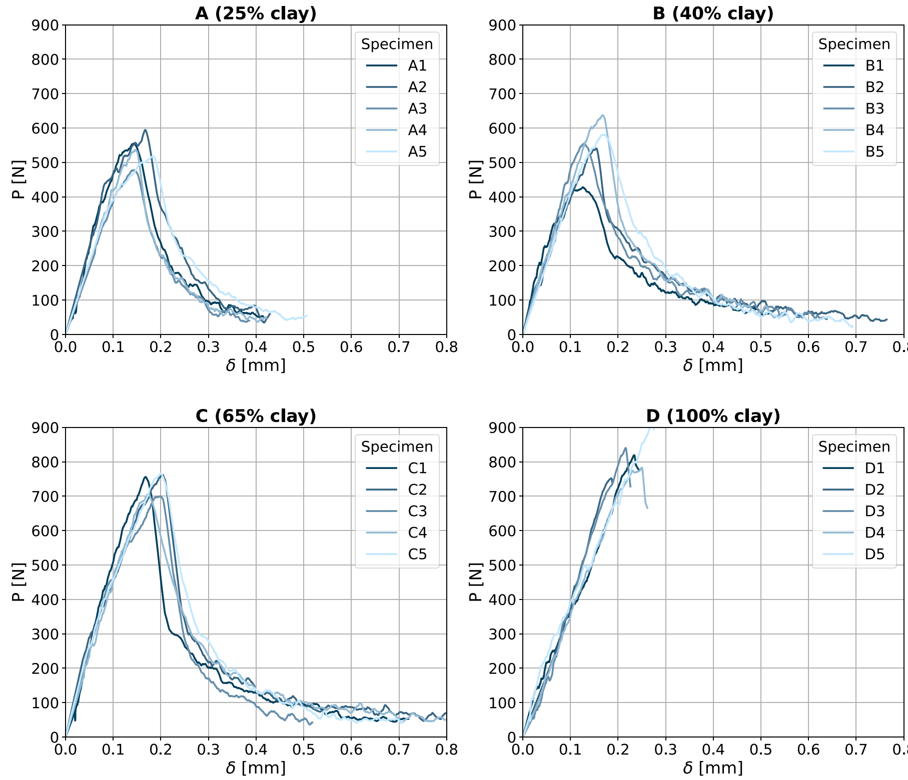

Fig. 3. Vertical load vs. vertical displacement at midspan (P–δ curves) obtained for RE series during 3PBT.

Table 2
Results from 3PBT.

Sample	ρ [kg/m^3]	P_{max} [N]	δ_p [mm]	δ_f [mm]	w_p [mm]	G_f^* [N/m]	G_f [N/m]
A1	2144	556	0.144	0.417	0.049	7.1	14.3
A2	2155	594	0.167	0.429	0.041	9.1	18.3
A3	2131	477	0.140	0.385	0.036	5.6	13.3
A4	2154	536	0.146	0.421	0.043	6.5	14.5
A5	2149	518	0.183	0.506	0.053	8.9	19.7
Mean A	2147	536	0.156	0.432	0.045	7.4	16.0
CV [%]	0.5	8.1	11.8	10.4	14.8	20.9	17.5
B1	2139	428	0.126	0.530	0.045	5.2	14.5
B2	2168	541	0.155	0.764	0.056	7.1	19.1
B3	2181	554	0.130	0.638	0.051	5.8	18.1
B4	2189	637	0.168	0.548	0.052	9.0	19.7
B5	2194	581	0.170	0.692	0.042	8.4	24.6
Mean B	2174	548	0.150	0.635	0.049	7.1	19.2
CV [%]	1.0	14.0	13.9	15.5	11.2	22.7	19.0
C1	2149	756	0.168	0.720	0.043	10.4	23.6
C2	2144	762	0.204	0.808	0.064	13.8	27.9
C3	2128	700	0.200	0.518	0.048	12.7	26.0
C4	2154	705	0.172	0.800	0.054	9.9	26.4
C5	2139	765	0.200	0.710	0.034	13.1	27.6
Mean C	2143	738	0.189	0.711	0.049	12.0	26.3
CV [%]	0.5	4.4	9.1	16.4	23.0	14.2	6.5
D1	2032	819	0.234	0.244	0.043	14.8	–
D2	2022	752	0.185	0.188	0.043	10.2	–
D3	2025	840	0.216	0.226	0.050	13.5	–
D4	2019	783	0.251	0.262	0.058	16.2	–
D5	2004	908	0.273	0.275	0.054	20.1	–
Mean D	2020	820	0.232	0.239	0.050	15.0	–
CV [%]	0.5	7.3	14.5	14.2	13.1	24.5	–

ρ: density; P_{max}: peak load; δ_p: vertical displacement at P_{max}; δ_f: vertical displacement at the end of the test; ω_p: notch opening at P_{max}; G_f: fracture energy; G_f^*: fracture energy at P_{max}.

ranged between 6.5% and 19.0% were obtained, a degree of dispersion that, while not negligible, aligns with (and in most cases is lower than) the values reported in the literature for RE materials. For instance, Arto et al. [12] reported coefficients of variation between 12% and 24% for comparable tests on lime-stabilized RE, while Corbin & Augarde [3] observed CV values as high as 55% for URE.

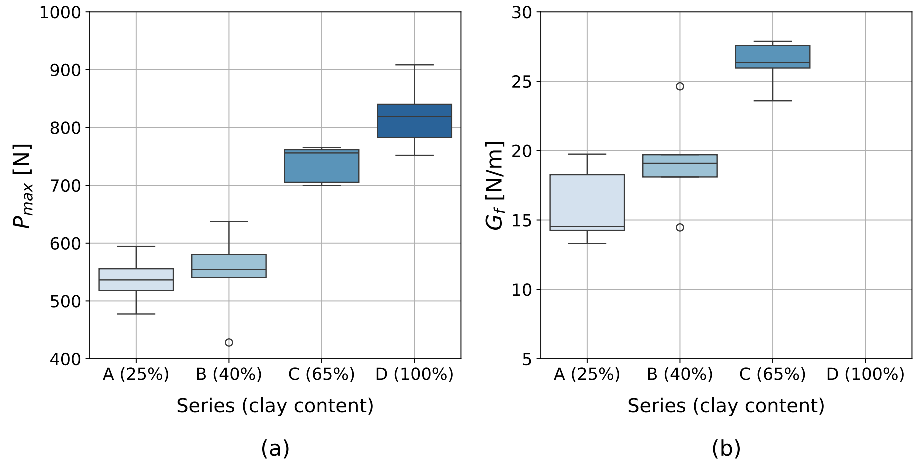

Fig. 4. Boxplots of the peak load (a) and fracture energy (b) obtained in the 3PBT.

Potential sources of variability include heterogeneity of the source soil, minor differences in specimen preparation, compaction uniformity, and coupling of sensors during NDT measurements. To mitigate these effects, the soil was carefully selected, sieved, and homogenized prior to specimen preparation. Standardized procedures were also applied, including the use of the Proctor method for compaction and careful sensor placement for FFRC and UPV tests, to further minimize variability.

However, and despite this (expected) variability, consistent patterns were observed across the different clay content series, allowing for meaningful interpretation of the influence of clay content on the fracture behavior of the RE samples. The main results from the 3PBT, in terms of peak load and fracture energy, are presented in Fig. 4. These plots clearly illustrate the trends in P_{max} and G_f, highlighting the improvements associated with increasing clay content. As previously noted, the total fracture energy of Series D samples could not be measured due to their sudden brittle fracture just after reaching the maximum load. While the number of specimens in the study was relatively limited (five per series), it is consistent with previous research in the field, and the low dispersion observed – compared to values reported in the literature – supports the adequacy of the sample size for capturing consistent and meaningful trends.

3.2. Prediction of the fracture behavior as a function of the clay content

Once the existence of a relationship between the clay content of URE and its fracture behavior has been established, it becomes useful to predict this behavior – expressed through the P–δ curve – as a function of the clay content. To this end, the P–δ curves were approximated using a piecewise function: a linear function for the hardening branch and an exponential function for the softening branch.

Although the most common approach to predict the fracture behavior of concrete is the bilinear softening law proposed by Hillerborg [36], a preliminary evaluation indicated that the exponential function could provide a better fit for the RE samples analyzed. Piecewise functions incorporating exponential softening have already been successfully used by other authors [33,41,42] for defining fracture P-δ curves of quasi-brittle materials.

The fitting procedure was carried out as follows:

1. A piecewise function, as defined in Eq. (3), was fitted for each series (A to D), yielding the parameters k, δ_p and α for each of the four clay contents considered. For Series D, only the linear ascending part of the function was considered. The coefficient of determination (R^2) was calculated for each fit.

$$P(\delta) = \begin{cases} k \cdot \delta & \text{if } \delta \leq \delta_p \\ k \cdot \delta_p \cdot \exp\left[-\alpha(\delta - \delta_p)^n\right] & \text{if } \delta > \delta_p \end{cases} \quad (3)$$

The exponent n was fixed at 0.7 to reduce the number of fitting parameters, as it was observed to accurately capture the shape of the softening branch across clay contents.

2. The fitting parameters (k, δ_p and α) were then expressed as linear functions of the clay content (c [%]), by performing a linear regression that minimized the combined fitting error across all four series. The resulting expressions are shown in Eq. (4):

$$\begin{aligned} k\,[\text{N/mm}] &= 0.25\,c + 3938.77 \\ \alpha\,[\text{mm}^{-1}] &= -0.0023\,c + 5.2860 \\ \delta_p\,[\text{mm}] &= 0.00128\,c + 0.10956 \end{aligned} \quad (4)$$

The values of the fitting parameters for the clay contents of RE series A to D are shown in Table 3.

3. Using these expressions, the fitting parameters were recalculated for the specific clay contents of 25, 40, 65 and 100% (Series A, B, C and D, respectively), and their corresponding P–δ curves were obtained using Eq. (3).

These results enable the prediction of the full fracture behavior of URE specimens as a function of clay content, including fracture energy, which can be computed from the area under the fitted P–δ curve. As shown in Fig. 5, excellent agreement was achieved between the experimental and fitted curves, with very high R^2 values for all series. This approach can also be used to estimate the fracture response for intermediate clay contents not directly tested in this study, or to complete the curve for Series D, whose softening branch could not be experimentally recorded due to sudden brittle failure.

The proposed piecewise linear-exponential modeling approach is consistent with widely used fracture models for quasi-brittle materials, such as concrete, where linear hardening followed by an exponential softening law is commonly adopted [33,41,42]. In the context of rammed earth, only one previous study [12] proposed a fitting curve for the P–δ fracture behavior, using an adjusted bilinear softening law, resulting broadly similar to the exponential softening adopted in the present study. As previously noted, no prior studies have proposed a predictive model linking fracture behavior or fracture energy directly to clay content in unstabilized rammed earth, making direct comparison impossible. Therefore, the present work provides both a robust description of the experimental curves and a novel methodology for extrapolating fracture properties as a function of clay content, complementing the scarce literature on URE fracture mechanics.

Table 3 summarizes the fitted parameters and the main fracture parameters for Series A to D. The proposed method accurately reproduces the fracture behavior of the samples, with limited deviations in the estimated peak load (slightly overestimated) and fracture energy (slightly underestimated). Somewhat larger discrepancies were observed for P_{max} of Series B, which exhibited higher variability in the

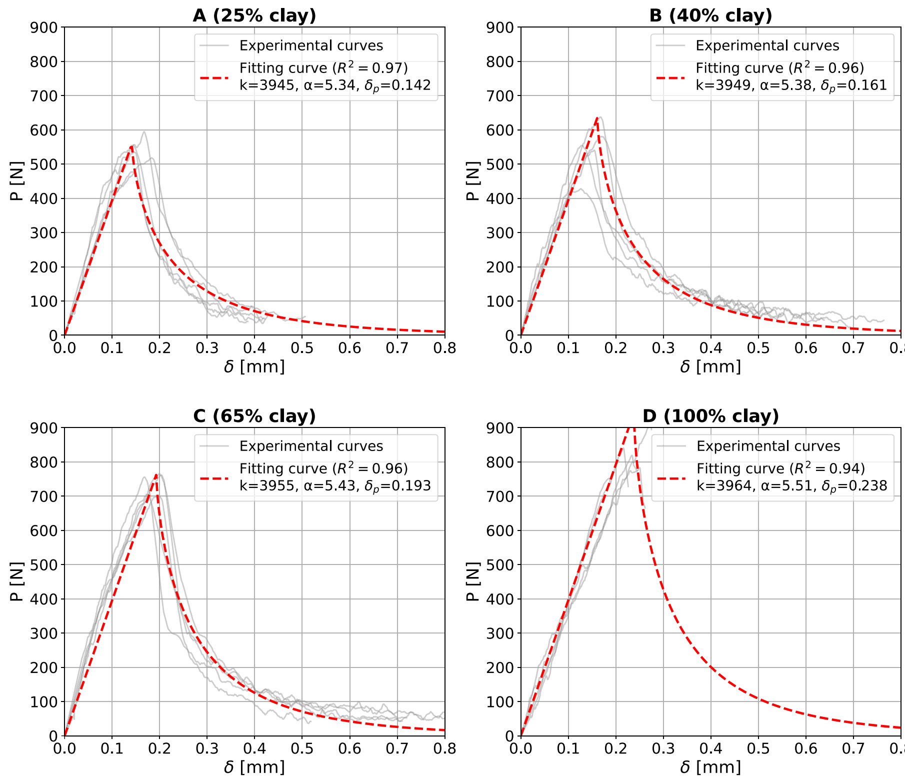

Fig. 5. Linear-exponential fitting for P–δ curves for Series A to D, as described by Eq. (3).

Table 3
Fitted fracture parameters and comparison with experimental results (percentage deviations shown in parentheses).

Parameter	Series A	Series B	Series C	Series D
k [N/mm]	3945.0	3948.8	3955.1	3963.8
α [mm^{-1}]	5.3431	5.3773	5.4344	5.5143
δ_p [mm]	0.142 (−9.3%)	0.161 (+7.4%)	0.193 (+2.1%)	0.238 (+2.6%)
P_{max} [N]	559 (+4.1%)	635 (+15.8%)	763 (+3.4%)	942 (+14.8%)
G_f [N/m]	15.9 (−0.7%)	19.1 (−0.5%)	25.0 (−4.9%)	34.4 (–)
G_f^* [N/m]	6.3 (−14.8%)	7.6 (+7.0%)	11.0 (−8.3%)	16.4 (+9.3%)
R^2 [%]	0.97	0.96	0.96	0.94

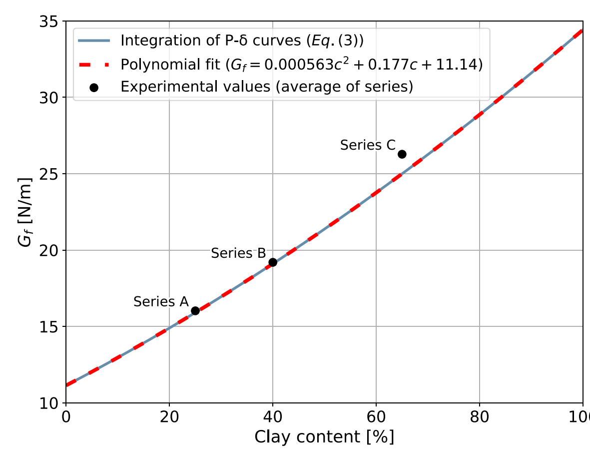

Fig. 6. Fracture energy as a function of clay content, result obtained by integrating the piecewise P-δ function (Eq. (3)) and its polynomial approximation.

peak load in the experimental results. The estimated fracture energy for Series D, which could not be determined experimentally, was found to be approximately 34 N/m.

According to the described methodology, fracture energy values in Table 3 were obtained by integrating the expression in Eq. (3) for each clay content. This relationship, representing G_f as a function of the clay content c, can be extended to all clay contents within the possible range (i.e., 0 to 100%), as shown in Fig. 6. Although the exact function $G_f(c)$ derived from the integration is quite complex and impractical for routine use, it can be accurately approximated by a polynomial function, as given in Eq. (5). This polynomial approximation is also illustrated in the referenced figure, demonstrating its precision (both functions are almost indistinguishable for the possible clay content range) and therefore its usability for practical applications.

$$G_f = 0.000563c^2 + 0.177c + 11.14 \quad (5)$$

The very high correlation levels observed in the analysis carried out in this study indicate that the overall fracture behavior – and in particular the fracture energy – of unstabilized rammed earth depends almost entirely on the clay content. This finding is highly valuable, as it simplifies the mechanical fracture characterization of rammed earth to an analysis of the clay content in the source material. The result is consistent with the fact that, in the case of unstabilized rammed earth, clay is essentially the only binding agent present.

3.3. Nondestructive assessment

The prediction of fracture properties through nondestructive techniques is particularly useful for RE, both in heritage structures – where destructive evaluation is typically not feasible –, and in new constructions, where producing test specimens with properties comparable to those of the actual walls is considerably more challenging than for conventional building materials such as concrete.

The results of the FFRC and UPV nondestructive tests on the RE specimens, performed immediately before the destructive 3PBT, are summarized in Table 4. An increase in both natural frequencies and

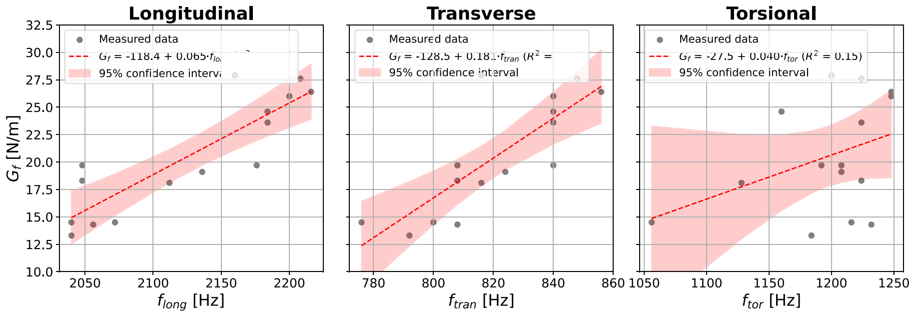

Fig. 7. Correlation between natural frequency obtained from FFRC tests and fracture energy.

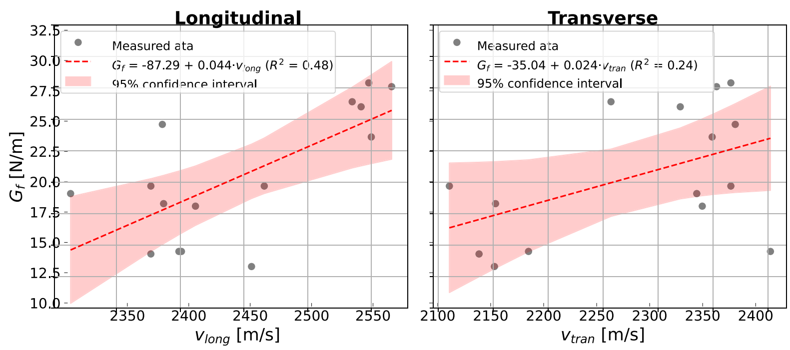

Fig. 8. Correlation between wave propagation velocity obtained from UPV tests and fracture energy.

Table 4
NDT results: mean and coefficient of variation (in parenthesis) of FFRC and UPV measurements for each clay content series.

Series	FFRC [Hz]			UPV [m/s]	
	f_{long}	f_{tran}	f_{tors}	v_{long}	v_{tran}
A	2053 (0.6%)	803 (0.9%)	1213 (1.5%)	2400 (1.4%)	2146 (1.2%)
B	2130 (2.7%)	819 (3.2%)	1149 (5.2%)	2395 (2.3%)	2362 (1.1%)
C	2194 (1.0%)	840 (1.8%)	1229 (1.6%)	2548 (0.4%)	2329 (1.9%)
D	2043 (1.3%)	805 (1.7%)	1104 (6.0%)	2351 (0.8%)	2084 (1.0%)

ultrasonic pulse velocities is observed with increasing clay content, with the only exception of pure clay samples (Series D), which show slightly lower values across all NDT parameters. In all cases, the measurements show very limited dispersion, suggesting that these methods can provide consistent indicators of material properties.

Linear regression was performed to evaluate the potential correlation between the NDT measurements and the fracture energy, identified as the most representative parameter for assessing the fracture behavior. Series D specimens were excluded from this analysis due to the absence of experimentally determined full G_f values, as previously described. Fig. 7 presents the fracture energy as a function of the longitudinal, transverse, and torsional natural frequencies measured through the FFRC tests. A reasonably strong linear correlation is observed for the longitudinal frequency, with a coefficient of determination of $R^2 = 0.75$. A moderate linear trend is also noted for the transverse mode – although with a lower coefficient of determination –, while no clear correlation appears to exist between fracture energy and the torsional frequency.

For the UPV test results, the relationship between fracture energy (G_f) and wave propagation velocity appears less defined (Fig. 8). A moderate correlation can be observed for the velocity measured along the longitudinal axis of the specimen (v_{long}), with a coefficient of determination $R^2 = 0.48$. However, the wave velocity in the transverse direction (v_{tran}) shows a much weaker correlation with G_f, indicating that this parameter may not be a reliable predictor of fracture energy in URE samples.

Taking a step further, combining nondestructive parameters from different tests can serve as a powerful approach to estimate the fracture properties of URE materials. In this context, the longitudinal natural frequency obtained from FFRC tests and the longitudinal wave velocity from UPV tests (values with the highest R^2 for each test) were used as input variables in a multivariable linear regression to predict the fracture energy of the specimens. While including squared and interaction terms could allow the model to account for curvature and interdependence between predictors – thereby capturing more complex relationships and potentially improving the fit – such complexity risks overfitting, especially given the relatively limited size of the dataset. Overfitting can reduce the generalizability of the model, as it may capture noise rather than meaningful trends.

Therefore, a simple linear regression model was adopted in this study, to ensure both interpretability and robustness of the results, favoring better generalization in future applications. Fig. 9(a) illustrates the resulting fitting surface for G_f as a function of the longitudinal natural frequency and longitudinal wave velocity, along with the corresponding experimental data. Fig. 9(b) presents the comparison between the experimentally obtained fracture energies and those predicted by the multivariable regression model. The results indicate that the combination of measurements from both NDT methods significantly improves the accuracy of the predictions, achieving a coefficient of determination of $R^2 = 0.80$.

To further assess the predictive performance of the regression models, Leave-One-Out Cross-Validation (LOOCV) was performed. This approach is well-suited for small datasets [43], as it iteratively trains the model on all samples except one and tests on the excluded sample, providing an internal validation metric. The LOOCV yielded a root mean square error (RMSE) of 2.85 N/m, corresponding to an average prediction deviation of 13% relative to the fracture energy values for samples not used in model fitting. This relatively low error indicates that the models effectively capture the main trends in the data and provides additional confidence in the predictive capability of the combined FFRC and UPV regression approach. Nevertheless, further testing with larger datasets would be beneficial to fully evaluate the generalizability of the models.

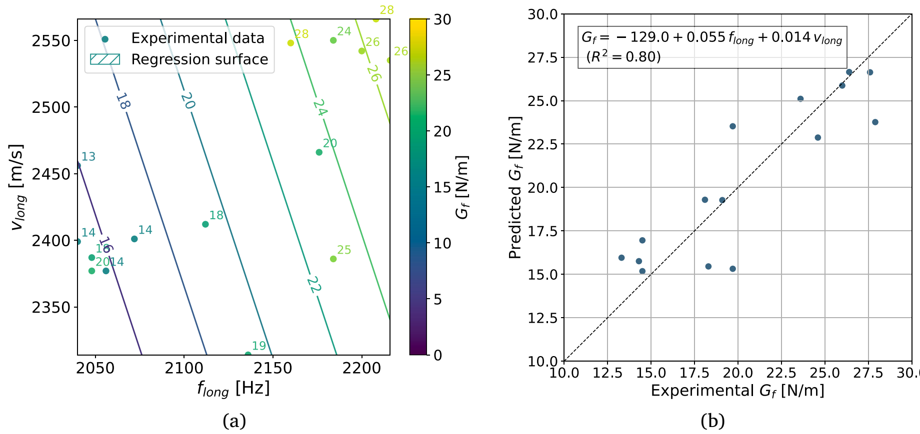

Fig. 9. Multivariable linear regression model predicting fracture energy as a function of longitudinal natural frequency and longitudinal wave velocity: (a) regression surface with experimental data points, and (b) comparison between predicted and experimental G_f values.

Additionally, a sensitivity analysis was performed to evaluate the influence of measurement uncertainties in the NDT data, arising from instrumental or environmental factors. For this purpose, an elasticity analysis was adopted, a standard approach in sensitivity assessment that quantifies the percentage change in a dependent variable caused by a 1% change in an independent variable [44]. Accordingly, the elasticity (e) of the fracture energy with respect to the longitudinal resonance frequency was defined as in Eq. (6) (with an analogous expression for the longitudinal UPV):

$$e(f_{\text{long}}) = \frac{f_{\text{long}}}{G_f} \cdot \frac{\partial G_f}{\partial f_{\text{long}}} \tag{6}$$

The analysis indicates that a 1% variation in the measured longitudinal frequency leads to an average variation of 5.6% in the estimated fracture energy, whereas the same variation in UPV results in a 1.6% change in G_f. These values suggest that the predictive model is moderately sensitive to measurement errors, particularly in resonance frequency, while being more robust with respect to UPV. This outcome highlights the importance of careful frequency determination in practical applications, but also confirms that the overall methodology remains reasonably stable in the presence of typical experimental uncertainties. In this study, precautions such as standardized sensor placement, consistent coupling conditions, and repeated measurements were applied to minimize dispersion, which further supports the reliability of the obtained correlations.

It should be noted, however, that the regression models for predicting fracture energy from NDT data were developed using laboratory specimens, manufactured under controlled conditions with relatively homogeneous material and compaction. In practice, full-scale or in-situ RE walls are likely to exhibit greater heterogeneity due to variations in soil properties, compaction uniformity, and construction techniques. Consequently, the predictive models presented here should be applied with caution to in-situ structures, and additional calibration or validation on full-scale walls is recommended to account for these sources of variability. Despite this limitation, the results provide a valuable baseline for nondestructive estimation of fracture properties and demonstrate that combining multiple NDT techniques can enhance predictive accuracy, with potential applicability to full-scale walls following proper calibration.

4. Conclusions

This study evaluates the fracture behavior of unstabilized rammed earth with varying clay contents through three-point bending tests, supported by nondestructive testing techniques. The results demonstrate a clear influence of clay content on the fracture behavior of the material. Increasing clay content leads to higher initial stiffness and peak load, with the most notable improvements observed in specimens containing 65–100% clay. However, for the pure clay series, a highly brittle behavior was observed, preventing the full characterization of the softening branch and total fracture energy due to sudden failure after peak load.

To facilitate broader applicability of the findings of the study, the load–displacement (P-δ) curves were approximated using a piecewise function – linear in the hardening phase and exponential in the softening phase – with fitting parameters expressed as functions of clay content. This allowed for predictive modeling of fracture behavior across a range of compositions, including an estimate of fracture energy for the pure clay series. Fracture energy, as a key indicator of the material's fracture behavior, showed meaningful trends across the tested series, with coefficients of determination over 0.94. The strong correlations found indicate that the fracture behavior – and especially the fracture energy – of unstabilized rammed earth is mainly controlled by clay content, a result consistent with clay being the primary binder in the material. This simplifies its mechanical characterization to assessing clay levels.

In terms of nondestructive assessment, both FFRC and UPV tests were performed, providing valuable insights for the evaluation of the fracture behavior. Longitudinal natural frequency from FFRC tests showed a strong correlation with fracture energy ($R^2 = 0.75$), while wave velocity measurements from UPV tests showed weaker but still interpretable trends, particularly if measured along the longitudinal axis of the specimen. Notably, combining these two NDT parameters in a multivariable linear regression significantly improved predictive power ($R^2 = 0.80$), underscoring the potential of hybrid nondestructive approaches for characterizing URE.

It should be noted that results presented in this study are based on specific local soils and standardized Proctor compaction. While the trends observed – such as the effect of increasing clay content on stiffness, peak load, and fracture energy – are expected to be generally applicable, absolute values may vary for different soils, climates, or compaction energies. Therefore, caution should be exercised when extrapolating the numerical results to other rammed earth materials.

Overall, the findings demonstrate the feasibility of accurately estimating fracture-related properties of URE based on clay content, supported by nondestructive measurements. This approach has practical implications for assessing and preserving existing earthen structures, particularly heritage buildings, where destructive testing is undesirable. A thorough understanding of how clay content influences fracture behavior – a key factor in RE failure – is essential for quality control and mix design in new rammed earth constructions. Nondestructive testing techniques are especially valuable for in-situ measurements, where obtaining representative samples can be challenging. Furthermore, the predictive models and NDT correlations can support seismic retrofitting, structural health monitoring, and material selection, providing engineers and practitioners with reliable tools to evaluate the mechanical performance of rammed earth constructions.

CRediT authorship contribution statement

Fernando Ávila: Writing – original draft, Visualization, Methodology, Investigation, Formal analysis, Data curation, Conceptualization. **Ricardo Castro:** Methodology, Investigation, Formal analysis, Data curation, Conceptualization. **Álvaro Blanca-Hoyos:** Methodology, Investigation, Formal analysis, Data curation, Conceptualization. **Rafael Gallego:** Writing – review & editing, Validation, Supervision, Funding acquisition, Conceptualization. **Esther Puertas:** Writing – review & editing, Validation, Supervision, Project administration, Funding acquisition, Conceptualization.

Declaration of competing interest

The authors declare that they have no known competing financial interests or personal relationships that could have appeared to influence the work reported in this paper.

Acknowledgments

This research is part of the project *"Evaluación de la vulnerabilidad estructural de patrimonio construido en tapia – VulTapia"* (Evaluation of the structural vulnerability of heritage built in rammed earth), funded by Consejería de Universidad, Investigación e Innovación, Spain and by ERDF Andalusia Program 2021–2027 [grant number C-ING-134-UGR23], developed in the Sustainable Engineering Structures Laboratory (SES-Lab) of the University of Granada. This study was partially supported by a doctoral grant to Álvaro Blanca-Hoyos within the program "*Formación de Investigadores — Contratos Predoctorales (FPU) Universidad de Granada–Banco Santander*". Special thanks are extended to Juan Blanco, MSc, for his valuable contributions to the conduction of the tests and the initial processing of the experimental data.

Data availability

Data will be made available on request.

References

[1] K. Barnaś, Earth-based construction: A critical review, Teka Kom. Urban. I Archit. Oddz. U Polskiej Akad. Nauk. W Krakowie (2022) http://dx.doi.org/10.24425/tkuia.2022.144860, URL https://journals.pan.pl/dlibra/publication/144860/edition/126499/content.

[2] F. Ávila, E. Puertas, R. Gallego, Characterization of the mechanical and physical properties of unstabilized Rammed Earth: A review, Constr. Build. Mater. 270 (2021) 121435, http://dx.doi.org/10.1016/j.conbuildmat.2020.121435.

[3] A. Corbin, C. Augarde, Fracture energy of stabilised Rammed Earth, Procedia Mater. Sci. 3 (2014) 1675–1680, http://dx.doi.org/10.1016/j.mspro.2014.06.270.

[4] V. Mora-Ruiz, J. Soto-Paz, S. Attia, C. Mejía-Parada, Sustainable earthen construction: A meta-analytical review of environmental, mechanical, and thermal performance, Buildings 15 (2025) 918, http://dx.doi.org/10.3390/buildings15060918.

[5] S. Samadianfard, V. Toufigh, Energy use and thermal performance of rammed-earth materials, J. Mater. Civ. Eng. 32 (2020) 4020276, http://dx.doi.org/10.1061/(ASCE)MT.1943-5533.0003364.

[6] S. Serrano, L. Rincón, B. González, A. Navarro, M. Bosch, L.F. Cabeza, Rammed Earth walls in mediterranean climate: Material characterization and thermal behaviour, Int. J. Low-Carbon Technol. (2016) 281–288, http://dx.doi.org/10.1093/ijlct/ctw022.

[7] A. Perić, I. Kraus, J. Kaluđer, L. Kraus, Experimental campaigns on mechanical properties and seismic performance of unstabilized Rammed Earth-A literature review, Buildings 11 (2021) 367, http://dx.doi.org/10.3390/buildings11080367.

[8] M.M. Hallal, S. Sadek, S.S. Najjar, Evaluation of engineering characteristics of stabilized rammed-earth material sourced from natural fines-rich soil, J. Mater. Civ. Eng. 30 (2018) 4018273, http://dx.doi.org/10.1061/(ASCE)MT.1943-5533.0002481.

[9] Q. Liu, L. Tong, Engineering properties of unstabilized Rammed Earth with different clay contents, J. Wuhan Univ. Technol. - Mater. Sci. Ed. 32 (2017) 914–920, http://dx.doi.org/10.1007/s11595-017-1690-y.

[10] F. Ávila, M. Fagone, R. Gallego, E. Puertas, G. Ranocchiai, Experimental and numerical evaluation of the compressive and shear behavior of unstabilized Rammed Earth, Mater. Structuctures 56 (2023) 118, http://dx.doi.org/10.1617/s11527-023-02206-9.

[11] T.T. Bui, Q.B. Bui, A. Limam, S. Maximilien, Failure of Rammed Earth walls: From observations to quantifications, Constr. Build. Mater. 51 (2014) 295–302, http://dx.doi.org/10.1016/j.conbuildmat.2013.10.053.

[12] I. Arto, R. Gallego, H. Cifuentes, E. Puertas, M.L. Gutiérrez-Carrillo, Fracture behavior of Rammed Earth in historic buildings, Constr. Build. Mater. 289 (2021) 123167, http://dx.doi.org/10.1016/j.conbuildmat.2021.123167.

[13] M.C.M. Parlato, C. Rivera-Gómez, S.M.C. Porto, Reuse of livestock waste for the reinforcement of rammed-earth materials: Investigation on mechanical performances, J. Agric. Eng. (2023) http://dx.doi.org/10.4081/jae.2023.1434.

[14] B. Mužíková, T.P. Otcovská, P. Padevět, Fracture energy of illitic Rammed Earth with high water-clay ratio, Acta Polytech. CTU Proc. 30 (2021) 53–57, http://dx.doi.org/10.14311/APP.2021.30.0053.

[15] S.M.S. Hussaini, V. Toufigh, Strength and fracture behavior of Rammed-Earth materials, J. Mater. Civ. Eng. 31 (2019) 1–13, http://dx.doi.org/10.1061/(ASCE)MT.1943-5533.0002876.

[16] L. Miccoli, D.V. Oliveira, R.A. Silva, U. Müller, L. Schueremans, Static behaviour of Rammed Earth: Experimental testing and finite element modelling, Mater. Struct. 48 (2015) 3443–3456, http://dx.doi.org/10.1617/s11527-014-0411-7.

[17] R. Silva, D. Oliveira, L. Schueremans, P. Lourenço, T. Miranda, Modelling the structural behaviour of Rammed Earth components, in: Civil-Comp Proc., Vol. 106, 2014, http://dx.doi.org/10.4203/ccp.106.112.

[18] P. Walker, R. Keable, J. Martin, V. Maniatidis, Rammed Earth: Design and construction guidelines, 2005.

[19] L. Xu, K.K. Wong, A. Fabbri, F. Champiré, D. Branque, Loading-unloading shear behavior of Rammed Earth upon varying clay content and relative humidity conditions, Soils Found. 58 (2018) 1001–1015, http://dx.doi.org/10.1016/j.sandf.2018.05.005.

[20] A. Khan, R. Gupta, M. Garg, Determining material characteristics of "Rammed Earth" using non-destructive test methods for structural design, Structures 20 (2019) 399–410, http://dx.doi.org/10.1016/j.istruc.2019.05.003.

[21] R. Liang, G. Hota, Y. Lei, Y. Li, D. Stanislawski, Y. Jiang, Nondestructive evaluation of historic hakka Rammed Earth structures, Sustainability 5 (2013) 298–315, http://dx.doi.org/10.3390/su5010298, URL https://www.mdpi.com/2071-1050/5/1/298.

[22] F. Ávila, E. Puertas, R. Gallego, Mechanical characterization of lime-stabilized Rammed Earth: Lime content and strength development, Constr. Build. Mater. 350 (2022) 128871, http://dx.doi.org/10.1016/j.conbuildmat.2022.128871.

[23] J.J.M. del Rio, J. Canivell, R.M. Falcón, The use of non-destructive testing to evaluate the compressive strength of a lime-stabilised rammed-earth wall: Rebound index and ultrasonic pulse velocity, Constr. Build. Mater. 242 (2020) http://dx.doi.org/10.1016/j.conbuildmat.2020.118060, 118060 Contents.

[24] F. Ávila, E. Puertas, J.M. Azañón, R. Gallego, Free-free resonance method for the mechanical characterization of carbonate rocks used as building stones, Mater. Constr. 72 (2022) e276, http://dx.doi.org/10.3989/mc.2022.03421.

[25] J.N. Eiras, Q.A. Vu, M. Lott, J. Payá, V. Garnier, C. Payan, Dynamic acousto-elastic test using continuous probe wave and transient vibration to investigate material nonlinearity, Ultrasonics 69 (2016) 29–37, http://dx.doi.org/10.1016/j.ultras.2016.03.008.

[26] F. Martínez-Soto, R. Gallego, E. Puertas, F. Ávila, Applicability of FFRC and SASW nondestructive techniques to assess the mechanical properties of concrete from early ages, in: Int. Conf. Constr. Energy, Environ. Sustain., Institute for Research and Technological Development for Construction, Energy, Environment and Sustainability (ITECOM), Funchal, Portugal, 2023.

[27] A. Guimond-Barrett, E. Nauleau, A.L. Kouby, A. Pantet, P. Reiffsteck, F. Martineau, Free-free resonance testing of in situ deep mixed soils, Geotech. Test. J. 36 (2013) 283–291, http://dx.doi.org/10.1520/GTJ20120058.

[28] K. Schaeffer, R. Bearce, J. Wang, Dynamic modulus and damping ratio measurements from free-free resonance and fixed-free resonant column procedures, J. Geotech. Geoenvironmental Eng. 139 (2013) 2145–2155, http://dx.doi.org/10.1061/(ASCE)GT.1943-5606.0000945.

[29] European Committee for Standardization (CEN), EN ISO 14688-2:2018. Geotechnical investigation and testing - identification and classification of soil - Part 2: Principles for a classification, 2018.

[30] ASTM, D1557-12R21 standard test methods for laboratory compaction characteristics of soil using modified effort (56,000 ft-lbf/ft3 (2,700 kn-m/m3)), 2021, http://dx.doi.org/10.1520/D1557-12.1.

[31] European Committee for Standardization (CEN), EN 14651:2005+A1:2007 Test method for metallic fibre concrete - Measuring the flexural tensile strength (limit of proportionality (LOP), residual), 2007.
[32] RILEM, Determination of the fracture energy of mortar and concrete by means of three-point bend tests on notched beams, Mater. Struct. 18 (1985) 287–290, http://dx.doi.org/10.1007/BF02472918.
[33] M. Elices, G.V. Guinea, J. Planas, Measurement of the fracture energy using three-point bend tests: Part 3—influence of cutting the P-δ tail, Mater. Struct. 25 (1992) 327–334, http://dx.doi.org/10.1007/BF02472591.
[34] ASTM, C215 standard test method for fundamental transverse, longitudinal, and torsional resonant frequencies of concrete specimens, 2019.
[35] European Committee for Standardization (CEN), EN 12504-4. Testing concrete in structures - part 4: Determination of ultrasonic pulse velocity, 2021.
[36] A. Hillerborg, The theoretical basis of a method to determine the fracture energyG F of concrete, Mater. Struct. 18 (1985) 291–296, http://dx.doi.org/10.1007/BF02472919.
[37] J. Planas, M. Elices, G.V. Guinea, Measurement of the fracture energy using three-point bend tests: Part 2—Influence of bulk energy dissipation, Mater. Struct. 25 (1992) 305–312, http://dx.doi.org/10.1007/BF02472671.
[38] Q.-B. Bui, T.-T. Bui, M.-P. Tran, T.-L. Bui, H.-A. Le, Assessing the seismic behavior of Rammed Earth walls with an L-form cross-section, Sustainability 11 (2019) 1296, http://dx.doi.org/10.3390/su11051296.
[39] FIB, CEB-FIP Model Code 90, Thomas Telford Ltd., London, UK, 1993.
[40] S. Lenci, F. Clementi, T. Sadowski, Experimental determination of the fracture properties of unfired dry earth, Eng. Fract. Mech. 87 (2012) 62–72, http://dx.doi.org/10.1016/j.engfracmech.2012.03.005.
[41] X. Liu, R. Duddu, H. Waisman, Discrete damage zone model for fracture initiation and propagation, Eng. Fract. Mech. 92 (2012) 1–18, http://dx.doi.org/10.1016/j.engfracmech.2012.04.019.
[42] K. Schrader, Hybrid 3D simulation methods for the damage analysis of multiphase composites (Ph.D. thesis), Bauhaus-Universität Weimar, Weimar, Germany, 2012, http://dx.doi.org/10.25643/bauhaus-universitaet.2059.
[43] M. Stone, Cross-validatory choice and assessment of statistical predictions, J. R. Stat. Soc. Ser. B Stat. Methodol. 36 (1974) 111–133, http://dx.doi.org/10.1111/j.2517-6161.1974.tb00994.x.
[44] K. Sydsæter, P.J. Hammond, Mathematics for Economic Analysis, Prentice Hall, New Jersey, USA, 1995, p. 982, URL https://www.ime.usp.br/~toscano/disc/calculo/SydsaeterHammondMathematicsforEconomicAnalysis.pdf.